Quantum transport in 3D Weyl semimetals: Is there a metal-insulator transition?

Klaus Ziegler[a]

Institut für Physik, Universität Augsburg, 86135 Augsburg, Germany

Abstract. We calculate the transport properties of three-dimensional Weyl fermions in a disordered environment. The resulting conductivity depends only on the Fermi energy and the scattering rate. First we study the conductivity at the spectral node for a fixed scattering rate and obtain a continuous transition from an insulator at weak disorder to a metal at stronger disorder. Within the self-consistent Born approximation the scattering rate depends on the Fermi energy. Then it is crucial that the limits of the conductivity for a vanishing Fermi energy and a vanishing scattering rate do not commute. As a result, there is also metallic behavior in the phase with vanishing scattering rate and only a quantum critical point remains as an insulating phase. The latter turns out to be a critical fixed point in terms of a renormalization-group flow.

1 Introduction

Since the discovery of the fascinatingly robust transport properties of graphene [1–4], there has been an increasing interest in other two-dimensional systems with similar spectral properties, such as the surface of topological insulators [5–9]. In all these systems the transport is dominated by a band structure, in which two bands touch each other at nodes. If the Fermi energy is exactly at or close to these nodes, the point-like Fermi surface and interband scattering lead to particular transport properties, such as a robust minimal conductivity. Based on these results, an extension of the nodal spectral structure to three-dimensional (3D) systems is of interest [10–30]. In 3D the Fermi surface is a sphere with radius $|E_F|$ rather than the circular Fermi surface in 2D, which is either occupied by electrons ($E_F > 0$) or by holes ($E_F < 0$). For $E_F = 0$ the conductivity vanishes in the absence of impurity scattering in contrast to the minimal conductivity of the 2D system. On the other hand, sufficiently strong impurity scattering leads to a conductivity at the node $E_F = 0$. Thus, an important difference between 2D and 3D Weyl fermions is that there exists a metal-insulator transition in the latter, which is driven by increasing disorder [27,29–33]. This transition is similar to the metal-insulator transition caused by decreasing random gap fluctuations in a system of 2D Dirac fermions [34–36]. On the other hand, it is quite different from an Anderson transition from a metallic state at weak scattering to an insulating state at strong scattering, which is caused by Anderson localization at strong scattering [37,38].

There is agreement between the various approaches, based on self-consistent, perturbative and numerical methods, on the existence of a transition from a 3D Weyl semimetal at weak scattering to a diffusive metallic behavior at stronger random scattering [10–33]. This transition can be characterized by a vanishing density of states at the Weyl node (i.e., the scattering rate or the imaginary part of the self-energy) and a nonzero density of states in the diffusive phase. However, the transport properties for the weak scattering regime are still under discussion. In particular, a recent study indicates that there is a metal-metal transition rather than a insulator-metal transition for 3D Weyl fermions with a critical point [30]. We will address this problem in the subsequent calculation, using a weak scattering approach (WSA).

Calculations of quantum transport consist usually of two steps: determining the scattering time (or scattering rate) within a self-consistent solution of the Dyson equation, also known as the self-consistent Born approximation (SCBA), and determining the conductivity by a self-consistent solution of the Bethe-Salpeter equation (BSE). This approach, in particular the solution of the BSE, is rather complex due to the existence of many modes. Not all of them are relevant for the transport properties because some decay quickly. From this point of view it is easier to project at the beginning only onto those modes which do not decay quickly but control the transport properties on large scales. For a system with spectral nodes in a disordered environment these modes are a result of a spontaneously broken chiral symmetry [39–42]. We will employ this idea here to 3D Weyl fermions in order to calculate the conductivity. For this purpose it is important to identify the underlying symmetries of the two-particle

[a] e-mail: ziegler@physik.uni-augsburg.de

Green's function. Then spontaneous symmetry breaking is characterized by its non-vanishing order parameter which is the scattering rate. There is a metallic phase with long range correlations (i.e. diffusion), whereas in the insulating phase the symmetry remains unbroken.

The paper is organized as follows: in Section 2 we define the model and discuss the symmetry properties of the two-particle Green's function. Then the DC conductivity is calculated within a weak scattering approach (Sect. 3), using an expansion in powers of the scattering rate η. This provides us a formula for the DC conductivity, which is discussed in Section 4 at the node (Sect. 4.1) and away from the node (Sect. 4.2). Our discussion includes a comparison with the results of the Boltzmann approach and with results from an approach based on the SCBA and BSE of references [26,30].

2 Model

The three-dimensional Weyl Hamiltonian for electrons with momentum $\boldsymbol{p}$ is expanded in terms of Pauli matrices τ_j $(j = 0, 1, 2, 3)$ as

$$H = v_F \boldsymbol{\tau} \cdot \boldsymbol{p} - U\tau_0 \quad \text{with} \quad \boldsymbol{\tau} = (\tau_1, \tau_2, \tau_3) \tag{1}$$

with Fermi velocity v_F. U is a disorder term, represented by a random potential with mean $\langle U \rangle = E_F$ (Fermi energy) and variance g. The average Hamiltonian $\langle H \rangle$ generates a spherical Fermi surface with radius $|E_F|$, and with electrons (holes) for $E_F > 0$ ($E_F < 0$). Physical quantities are expressed in such units that $v_F \hbar = 1$.

The electronic conductivity, obtained as the response to a weak external field with frequency $\omega \sim 0$ [4,43,44]

$$\sigma(\omega) = -\frac{e^2}{2h}\omega^2 \sum_r r_k^2 A_{r0}(\omega), \tag{2}$$

is given by the correlation function of the Green's functions $(H \pm z)^{-1}$

$$A_{rr'}(\omega) = \lim_{\epsilon \to 0} \langle Tr_2[(H+z)^{-1}_{rr'}(H-z)^{-1}_{r'r}] \rangle \tag{3}$$

with

$$z = \omega/2 + i\epsilon,$$

where $\langle \ldots \rangle$ represents disorder average and Tr_2 is the trace with respect to the Pauli matrix structure. This expression, often called the two-particle Green's function, has two different energies $\pm z$ for the same Hamiltonian H to create two independent Green's functions $(H \pm z)^{-1}$. Now we represent this two-particle Green's function by two different Hamiltonians and one energy: we define the pair of Hamiltonians

$$H_\pm = p_1\tau_1 + p_2\tau_2 \pm (p_3\tau_3 - U\tau_0), \tag{4}$$

where $H_+ = H$. The matrix transposition ^{T} relates H_+ and H_- through the identity

$$\tau_1 H_\pm^T \tau_1 = -H_\mp, \tag{5}$$

since $p_j^T = -p_j$. This allows us to write for the correlation function (3)

$$A_{rr'}(\omega) = -\lim_{\epsilon \to 0} \left\langle Tr_2[(H_+ + z)^{-1}_{rr'} \tau_1 (H_-^T + z)^{-1}_{r'r} \tau_1] \right\rangle . \tag{6}$$

Instead of two different energies $\pm z$ and the same Hamiltonian H, the two-particle Green's function has now the same energy z but different Hamiltonians, namely H_+ and H_-^T. The relation (5) and the representation (6) reveals an internal structure of the model which leads to the Hamiltonian

$$\hat{H} = \begin{pmatrix} H_+ & 0 & 0 & 0 \\ 0 & H_- & 0 & 0 \\ 0 & 0 & H_-^T & 0 \\ 0 & 0 & 0 & H_+^T \end{pmatrix}. \tag{7}$$

The Green's functions $(H_+ + z)^{-1}$ and $(H_-^T + z)^{-1}$ in equation (6) are just the first and the third diagonal element of the Green's function $(\hat{H} + z)^{-1}$. This indicates that the transport properties of the original Hamiltonian H, which requires two different energies $\pm z$, are related to the transport properties of the extended Hamiltonian $\hat{H}$ at the same energy z.

The extended Hamiltonian $\hat{H}$, its symmetries and its relation to diffusive transport were studied previously [39–42,45]. In particular, it was found, together with property (5), that the matrix

$$\hat{S} = \begin{pmatrix} 0 & 0 & \varphi_1\tau_1 & 0 \\ 0 & 0 & 0 & \varphi_2\tau_1 \\ \varphi_1'\tau_1 & 0 & 0 & 0 \\ 0 & \varphi_2'\tau_1 & 0 & 0 \end{pmatrix} \tag{8}$$

with scalar variables φ_j, φ_j' anticommutes with $\hat{H}$: $\hat{S}\hat{H} = -\hat{H}\hat{S}$. This relation implies a non-Abelian chiral symmetry [39–41]:

$$e^{\hat{S}} \hat{H} e^{\hat{S}} = \hat{H} \tag{9}$$

which is a symmetry relation for the extended Hamiltonian $\hat{H}$ in equation (7). The term proportional to z in the Green's function $\hat{G}(z)$ breaks this symmetry due to $e^{\hat{S}} \neq \mathbf{1}$, and therefore, $\lim_{z\to 0}[\hat{G}(z) - \hat{G}(-z)]$ plays the role of an order parameter for spontaneous symmetry breaking:

$$\hat{G}(z) - \hat{G}(-z) = -2z\hat{G}(z)\hat{G}(-z) = -2z(\hat{H}^2 - z^2)^{-1}. \tag{10}$$

Since the diagonal elements of this expression are proportional to the density of states at the node when we take the limit $z \to 0$, a non-vanishing density of states indicates spontaneous symmetry breaking. The role of a non-vanishing density of states at the node as an order parameter for a diffusive metallic phase was also discussed in references [24,29,31].

Following the recipe of references [40,41] the correlation function (6) can be expressed as a diffusion propagator. This is used in the next section, where we focus on the long-range behavior of $A_{rr'}(\omega)$ to calculate the conductivity $\sigma(\omega)$.

3 Weak-scattering approach

The scattering rate η is defined by

$$\eta = \frac{i}{2}\frac{Tr[\langle (H+i\epsilon)^{-1}\rangle - \langle (H-i\epsilon)^{-1}\rangle]}{Tr[\langle (H+i\epsilon)^{-1}\rangle\langle (H-i\epsilon)^{-1}\rangle]}. \tag{11}$$

This definition is motivated by the assumption of a complex self-energy for the average one-particle Green's function $\langle (H+i\epsilon)^{-1}\rangle$, whose imaginary part is the scattering rate (cf. Appendix A). The corresponding scattering time τ is $\tau = \hbar/\eta$. η can either be calculated, for instance, within the SCBA [4,31,32] or it can be taken from experimental measurements. As discussed in the previous section, a non-vanishing scattering rate indicates spontaneous symmetry breaking. Since the broken symmetry is continuous, there exists a massless mode. The latter is reflected by the relation

$$\begin{aligned}\sum_{r'} A_{rr'}(\omega) &= Tr_2\langle [(H+\omega/2)^{-1}(H-\omega/2)^{-1}]_{rr}\rangle \\ &= -\frac{1}{\omega}Tr_2[\langle (H+\omega/2)^{-1}_{rr}\rangle - \langle (H-\omega/2)^{-1}_{rr}\rangle]\end{aligned} \tag{12}$$

which diverges for a vanishing symmetry breaking term $\omega \sim 0$ due to long-range correlations. For the correlation function (6) a similar but more elaborate analysis yields a diffusion propagator [34,35], whose Fourier components read

$$\tilde{A}_q(\omega) \approx -\frac{\eta}{g}\frac{1}{i\omega/2 + Dq^2}. \tag{13}$$

This agrees with (12) for $q = 0$ when we use the self-consistent approximation $\langle (H+i\epsilon+\omega/2)^{-1}_{rr}\rangle \approx -\Sigma/g$ of Appendix A. This is not an accident but a consequence of the fact that the self-consistent approximation represents the saddle point of the corresponding functional integral [40,41]. The prefactor of the q^2 term is the diffusion coefficient

$$D = \frac{g\eta}{2}\int_k Tr_2\left(\frac{\partial(\langle H\rangle + i\eta)^{-1}}{\partial k_l}\frac{\partial(\langle H\rangle - i\eta)^{-1}}{\partial k_l}\right). \tag{14}$$

Thus, the DC limit $\omega \to 0$ of the conductivity formula in (2) and the correlation function (13) reproduce the Einstein relation

$$\sigma = \frac{e^2}{h}\frac{2\eta}{g}D, \tag{15}$$

which gives with the right-hand side of equation (14) for 3D Weyl fermions the integral

$$\begin{aligned}\sigma(\eta, E_F) = 2\frac{e^2}{h}\eta^2 &\\ \times \int_0^\lambda \frac{(\eta^2+k^2)^2 + E_F^2(2\eta^2+2k^2/3+E_F^2)}{[(\eta^2-E_F^2+k^2)^2+4\eta^2E_F^2]^2} &\\ \times \frac{k^2dk}{2\pi^2}&\end{aligned} \tag{16}$$

with momentum cut-off λ. Thus, the conductivity depends on the disorder strength g only through the scattering rate η.

A diffusion propagator can also be calculated from the BSE, as demonstrated recently for 3D Weyl fermions [26,30]. However, the derivation of the propagator (13) from the symmetry (9) has the advantage that it is simpler and that we obtain the diffusion coefficient D in equation (14) directly as a quadratic form of Green's functions.

4 Results and discussion

In the following we present and discuss the results which are obtained from the conductivity $\sigma(\eta, E_F)$ in equation (16). This expression is subtle in the limit of a vanishing scattering rate η, since the latter appears as η^2 in front of an integral that diverges for $\eta \to 0$. This makes the conductivity very sensitive to the order of the limits $E_F \to 0$ and $\eta \to 0$ in the case when the scattering rate vanishes at the node. Since the conductivity depends on η and E_F separately, we consider first properties exactly at the node $E_F = 0$, where results are simple, and then the more complex results when η depends on E_F. For the second part we employ the SCBA to determine the function $\eta(E_F)$ and calculate the corresponding conductivity.

4.1 Transport at the spectral node

At the node ($E_F = 0$) the DC conductivity in equation (16) is reduced to the expression

$$\begin{aligned}\sigma &= 2\frac{e^2}{h}\eta^2\int_0^\lambda \frac{k^2}{(\eta^2+k^2)^2}\frac{dk}{2\pi^2} \\ &= \frac{e^2\eta}{2\pi^2 h}\left[\arctan(1/\zeta) - \frac{\zeta}{1+\zeta^2}\right] \quad (\zeta = \eta/\lambda),\end{aligned} \tag{17}$$

which becomes for $\lambda \gg \eta$

$$\sigma \sim \frac{e^2}{4\pi h}\eta. \tag{18}$$

In contrast to the 2D case, where $\sigma = e^2/\pi h$, the 3D case gives a linearly increasing behavior with respect to the scattering rate. This result was derived directly (i.e., without using Eq. (16)) by Fradkin some time ago [10]. With a disorder dependent scattering rate he also obtained a transition for a critical disorder strength g_c, where the conductivity vanishes for $g \le g_c$ and increases linearly for $g > g_c$.

The linear behavior indicates an unconventional transport because in the classical Boltzmann approach for one-band metals the conductivity *decreases* with increasing scattering rate: $\sigma_B = ne^2/m\hbar\eta$ (n: electron density, m: electron mass) [46]. This remains true when we include the band structure of the Weyl fermions in the Boltzmann approach: σ_B is nonzero at the node for any scattering rate and even diverges with vanishing disorder as [30]

$$\sigma_B = \frac{1}{2\pi}\frac{e^2v_F^2\hbar}{g}, \tag{19}$$

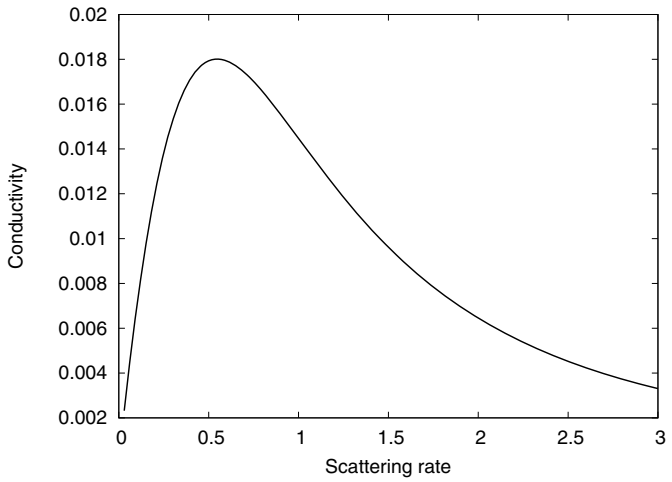

Fig. 1. The conductivity of 3D Weyl fermions (16) as a function of the scattering rate η at Fermi energy $E_F = 0$. It describes the crossover from the quantum regime for $\eta < 0.6$ to the classical Boltzmann regime for $\eta > 0.6$.

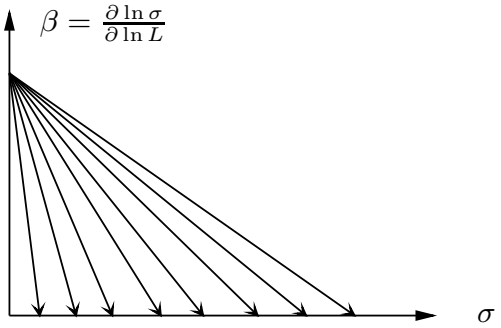

Fig. 2. The β-function for different scattering rates, where the arrows indicate the flow toward the fixed points. The β-function increases with η and creates a line of fixed points $\sigma^* \sim \eta e^2/4h\pi$. This plot is based on an approximation near the fixed points according to equation (21).

where g is related to the density of impurities n_i and the impurity potential u_0 by the equation $g = n_i u_0^2$ [30]. The disagreement between the expressions in (17) and (19) can be explained by interband scattering, caused by particle-hole creation processes, which has been ignored in the Boltzmann approach. On the other hand, the increasing behavior of (17) for small η turns into a decreasing behavior for larger η, as one can see in Figure 1, indicating a crossover from quantum transport for weak scattering to conventional Boltzmann transport for stronger scattering.

In this context it is also interesting to study the finite-size effects of the conductivity by considering a cubic system of finite length L. The β-function $\beta = \partial \ln \sigma / \partial \ln L$ describes the finite-size scaling of the conductivity. It can be calculated from equation (16) by replacing the lower integration boundary with $1/L$, which assumes non-periodic boundary conditions. Then $\sigma(\eta, L)$ in equation (17) is a monotonically increasing function for increasing size L with

$$\sigma(\eta, L) \sim \sigma^* - \frac{e^2}{h} \frac{\eta}{(L\eta)^2} \tag{20}$$

for $L\eta \gg 1$, where σ^* is the expression (18). The corresponding β-function reads

$$\beta \sim 2[1 - \sigma(\eta, L)/\sigma^*], \tag{21}$$

which vanishes at the η-dependent fixed point σ^*. This differs from the 2D case only by different fixed points σ^*, where in 2D it is a universal constant $\sigma^* = e^2/\pi h$ [47] and in 3D it is the η-dependent expression (18).

It should be noticed that σ^* is not a critical point because it is an attractive fixed point. But since for 3D Weyl fermions σ^* depends on the scattering rate η, we have a line of fixed points for $\eta \geq 0$. Thus, the endpoint $\sigma^* = 0$ for $\eta = 0$ has the feature of a critical point because any change of η drives us away from this endpoint, as illustrated in Figure 2. It indicates a transition from an insulator ($\eta = 0$) to a metal ($\eta > 0$). The transition is driven by increasing disorder, since the scattering rate is a monotonic function of the disorder strength g. η is also the order parameter for spontaneous symmetry breaking (10), which can be calculated from equation (11) within SCBA. From the solution of the self-consistent equation (A.6) we get for $\gamma = g/2\pi^2$ and $\eta \sim 0$ the linear behavior

$$\eta \sim \frac{2\lambda}{\pi} (\lambda\gamma - 1)\, \Theta(\lambda\gamma - 1) \quad (\gamma = g/2\pi^2) \tag{22}$$

with the step function Θ. For $\gamma \leq \gamma_c = 1/\lambda$ we have no spontaneous symmetry breaking. Thus, η as well as the DC conductivity vanish strictly. When we approach γ_c from above there is linear behavior for the scattering rate, which agrees with the numerical calculation of Kobayashi et al. [29]. At the critical point itself we obtain from the Einstein relation (15) a finite diffusion coefficient

$$D(g_c) \approx \frac{g_c e^2}{4\pi}.$$

The results of the DC conductivity from previous self-consistent studies, based on a combination of SCBA and a self-consistent solution of the BSE [26,30], are summarized and compared with our results of the WSA in Table 1. For sufficiently large scattering rates the Boltzmann approach, the solution of the BSE and the result of the WSA agree reasonably well, reflecting a rather conventional transport. This indicates that quantum effects, such as particle-hole pair creation, are dominated by impurity scattering. On the other hand, for smaller values of the scattering rate the conductivity exhibits a larger variety of results: the Boltzmann conductivity has a simple $1/g$ behavior, which is also found with the solution of the BSE in reference [26], with a different constant prefactor though. In contrast, the approximative analytic solution of the BSE in reference [30] has a characteristic dip down to zero at a critical g_c and increases for $g > g_c$ and for $g < g_c$:

$$\sigma = \sigma_1 |1/g - 1/g_c|, \quad \sigma_1 = \bar{\sigma} \begin{cases} 1 & \text{for } g < g_c \\ 3 & \text{for } g > g_c. \end{cases} \tag{23}$$

When we compare this result with the WSA conductivity in equation (17) it should be noticed that the latter

Table 1. The scattering rate η and the conductivity at the node calculated with three different methods. The translation from reference [30] is $g = n_i u_0^2$ and the SCBA coefficient σ_1 is given in equation (23).

At the node	Boltzmann approach [30]	SCBA & BSE [26]	SCBA & BSE [30]	SCBA & WSA
Scattering rate η	0	0	$2(g/g_c - 1)/\pi$	$2(g/g_c - 1)/\pi$
Conductivity σ	$e^2 v_F^2 \hbar/2\pi g$	$4e^2 v_F^2/gh$	$\sigma_1 e^2/4\pi h$	Eq. (17), Fig. 1
Away from the node $g < g_c$				
Scattering rate η	$\propto E_F^2$	$\hbar g E_F^2/8\pi v_F^3$	$E_F g_c/(g_c - g)$	Eq. (24)
Conductivity σ	$\sigma_B(0)(1 + 6E_F^2/E_0^2)$	$4e^2 v_F^2/gh$	$\propto E_F g_c/(g_c - g)$	Fig. 4

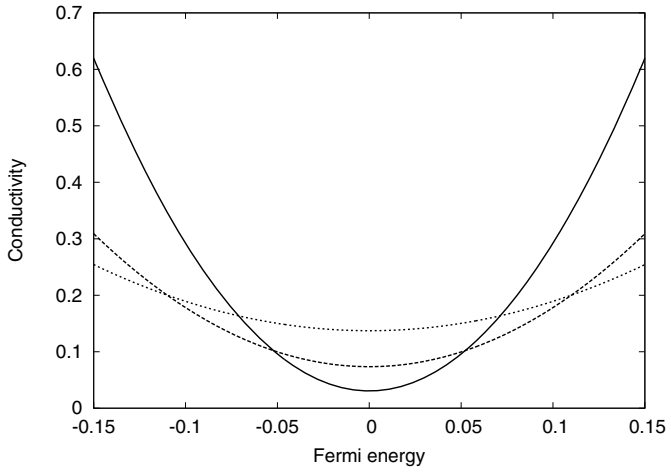

Fig. 3. The conductivity (16) as a function of the Fermi energy E_F at fixed scattering rates $\eta = 0.02$ (full curve), $\eta = 0.05$ (dashed curve) and $\eta = 0.1$ (dotted curve).

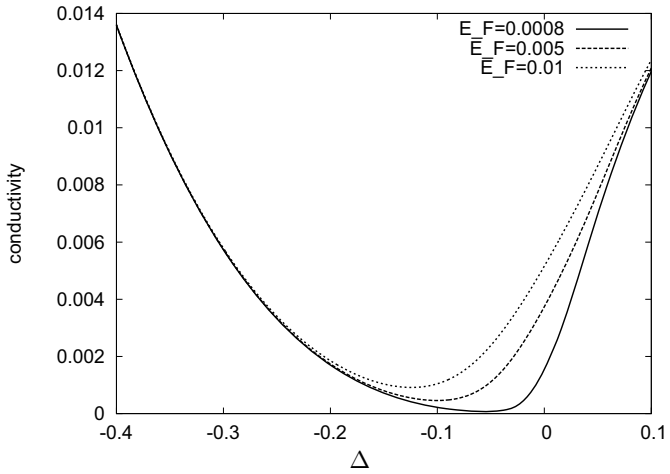

Fig. 4. The conductivity (16) as a function of the disorder parameter $\Delta = \gamma\lambda - 1$ with a self-consistent scattering rate $\eta(\Delta)$ for different values the Fermi energy E_F. The curves tend to reach the critical point $\Delta = 0$ by a sharp cusp as the Fermi energy approaches the node $E_F = 0$. Further away from the critical point the conductivity is much less sensitive to a change of E_F.

was obtained by sending $E_F \to 0$ first and then $\eta \to 0$. As mentioned at the beginning of this section the value of the conductivity depends on the way we take these two limits. Although nothing has been said in reference [30] about the order of the two limits to get (23), we will study in Section 4.2 the case when E_F and η go to zero simultaneously in equation (16). Then we obtain a result similar to (23).

4.2 Transport away from the spectral node

The conductivity as a function of the Fermi energy is plotted at fixed scattering rates in Figure 3. As we increase the scattering rate the effect of the node is washed out and the conductivity becomes flatter. This is similar to the behavior in Figure 1. In other words, impurity scattering supports transport near the node whereas it suppresses it further away. Thus, we can distinguish a regime close to the node, where the conductivity increases with the scattering rate, and a more conventional regime further away from the node, where the conductivity decreases with the scattering rate, as also described by the Boltzmann approach.

So far we have considered the case that η and E_F are independent. However, in general the scattering rate depends on γ and E_F. For instance, the self-consistent calculation in Appendix A, based on the SCBA or saddle-point approximation, creates a scattering rate in equation (A.4) that depends on the Fermi energy:

$$\eta = Re\left[\frac{(\gamma\lambda - 1)}{\gamma\pi} + \sqrt{\frac{(\gamma\lambda - 1)^2}{\gamma^2\pi^2} - \frac{2iE_F}{\gamma\pi}}\right]. \qquad (24)$$

The behavior of the conductivity in (16) is affected by this result, since the limits $\eta \to 0$ and $E_F \to 0$ are not independent anymore. Equation (24) has two typical regimes, namely $\eta \propto E_F$ near the critical point $\gamma\lambda = 1$, which leads to $\sigma \propto E_F$, and $\eta \propto E_F^2$ for $\gamma\lambda \ll 1$, which leads to a non-vanishing conductivity for $E_F \to 0$. This implies that the conductivity vanishes only for $\gamma\lambda \sim 1$, whereas it nonzero above and below $\gamma\lambda \sim 1$. Thus, there is no insulating phase but only an insulating point for $\gamma\lambda = 1$, in agreement with the analytic result of reference [30]. The behavior of the conductivity as a function of $\gamma\lambda - 1$ is plotted for different values of the Fermi energy in Figure 4. It should be noticed, though, that the transport behavior is determined by the E_F dependence of the scattering rate of the special form in equation (24). Using another form of the scattering rate as a function of the Fermi energy can lead to a substantially different behavior of the conductivity near the node. An example was observed in reference [30] within a numerical solution of the SBCA and the BSE, where the scattering rate is exponentially small

for $\gamma < \gamma_c$. In this case a vanishing conductivity was found at the node also for $\gamma < \gamma_c$.

5 Conclusions

We have studied the DC conductivity of 3D Weyl fermions in the presence of random scattering. The relevant parameters in the conductivity (16) are the scattering rate η, which is an order parameter for spontaneous chiral symmetry breaking, and the Fermi energy E_F. Exactly at the node $E_F = 0$ there is a metal-insulator transition with a diffusive metal for $\eta > 0$ and an insulator for $\eta = 0$. The conductivity is linearly increasing with η up to a maximal value and decreases for stronger scattering rates, as illustrated in Figure 1. This non-monotonic behavior is in contrast to the constant conductivity in the corresponding 2D system. It reflects the fact that the increased phase space of the 3D Weyl fermions suppresses the conductivity for weak scattering but also that stronger scattering implies a screening of the node such that the Boltzmann approach eventually becomes applicable. Further away from the node the behavior depicted in Figure 3 agrees qualitatively with that of the 2D system [42], which was also obtained in a quasiclassical approach [48]. The latter diverges as one approaches the node, which indicates that the full quantum approach is necessary near the node.

The critical behavior at the node describes an unconventional phase transition for $\gamma = \gamma_c$ which is driven by quantum fluctuations: in contrast to a conventional transition the symmetry broken phase with $\eta > 0$ is characterized by robust diffusion whereas the phase with unbroken symmetry ($\eta = 0$) has a subtle behavior in terms of the conductivity because it is very sensitive to the limit $E_F \to 0$. Thus, it is possible that we either have an insulating phase with vanishing conductivity when the scattering rate vanishes slowly with E_F or a metallic phase when the scattering rate vanishes sufficiently fast with E_F. In the case of an SCBA calculation for η there is only a quantum critical point in the transport properties and metallic behavior above and below this critical point. It cannot be ruled out, though, that a different calculation of η leads to a different behavior. Thus, our discussion of the delicate limits $\eta, E_F \to 0$ clarifies some of the contradicting results in the literature about the presence of a metal-insulator transition for 3D Weyl fermions [26,30]. Moreover, the fact that the conductivity depends only on η and E_F allows us to determine η independently with other approximations than the SCBA, and to insert the result into the conductivity (16). A possible step in this direction is a correction to the SCBA [32] or perturbative renormalization-group approach in $d-2$-expansion. The latter gives $\eta(E) \propto E^{1.3}$ [29,31]. This result would lead to a vanishing conductivity below the critical point.

In the regime $0 < \gamma < \gamma_c$ disorder may also affect physical properties of Weyl fermions in another way. The reason is the existence of non-uniform solutions of the SCBA with an exponentially small contributions to η, similar to Lifshitz tails in the density of states of disordered systems [49]. In the case of 2D Weyl fermions this has been discussed in reference [50]. The problem, however, is always that the self-consistent equation is nonlinear and has many non-uniform solutions. Under certain plausible assumptions for the solutions η, the existence of exponentially small contributions for $\gamma < \gamma_c$ has been discussed for 3D Weyl fermions in reference [24]. The corresponding states might be localized then with no contribution to the conductivity at $T = 0$. However, for $T > 0$ thermally activated electrons may hop between patches of localized states and provide a hopping conductivity [51]. Whether or not resonant tunneling without spontaneous symmetry breaking can occur in this case is an open question.

I am grateful to David Schmeltzer for an extended discussion of Weyl fermions.

Appendix A: Self-consistent approximation

The first step is to study spontaneous symmetry breaking of the symmetry (9) by a non-zero scattering rate within SCBA, following a similar approach as given in reference [30]. The average one-particle Green's function then reads

$$\langle (H+z)^{-1} \rangle \approx (\langle H \rangle + z + \Sigma)^{-1}, \tag{A.1}$$

and the self-energy is given by

$$\Sigma = -g(\langle H \rangle + \Sigma + i\epsilon)^{-1}. \tag{A.2}$$

The imaginary part of the self-energy Σ is a scattering rate η. Then the self-energy reads in our case with the momentum cut-off λ

$$\Sigma = \gamma\alpha \left[\lambda - \frac{\alpha}{2} \log\left(\frac{\alpha+\lambda}{\alpha-\lambda} \right) \right] \quad (\gamma = g/2\pi^2, \quad \alpha = E_F + \Sigma). \tag{A.3}$$

For small E_F near the node we expand equation (A.3) in powers of α up to second order to obtain

$$\Sigma \sim -E_F + \frac{i(\gamma\lambda - 1)}{\gamma\pi} + i\sqrt{\frac{(\gamma\lambda-1)^2}{\gamma^2\pi^2} - \frac{2iE_F}{\gamma\pi}}. \tag{A.4}$$

The real part of Σ provides a shift of the Fermi energy:

$$\Sigma \sim -E_F + i\sqrt{-\frac{2iE_F}{\gamma\pi}} = -E_F + e^{i\pi/4}\sqrt{\frac{2E_F}{\gamma\pi}}, \tag{A.5}$$

where the sign is chosen such that we have a positive scattering rate.

At the node $E_F = 0$ the self-consistent equation (A.3) reduces to $\eta = \eta I$ with

$$I = \gamma \left[\lambda - \eta \arctan(\lambda/\eta) \right].$$

There are two solutions, namely $\eta = 0$ and $\eta \neq 0$ with

$$\lambda\gamma = \frac{1}{1 - \zeta \arctan(1/\zeta)}, \qquad \zeta = \eta/\lambda. \tag{A.6}$$

A nonzero η reflects spontaneous symmetry breaking with respect to equation (9). Such a solution exists for equation (A.6) only at sufficiently large γ. Moreover, η vanishes continuously as we reduce γ. A nonzero η is proportional to the density of states at the Fermi level. However, even for $\eta = 0$ there can be a nonzero local density of states due to localized energy levels, which are not counted in η within the SCBA. For $\zeta \sim 0$ we obtain the linear behavior

$$\zeta \sim \frac{2}{\pi}(\gamma\lambda - 1).$$

References

1. K.S. Novoselov et al., Nature **438**, 197 (2005)
2. Y. Zhang, Y.-W. Tan, H.L. Stormer, P. Kim, Nature **438**, 201 (2005)
3. A.H. Castro Neto, F. Guinea, N.M.R. Peres, K.S. Novoselov, A.K. Geim, Rev. Mod. Phys. **81**, 109 (2009)
4. D.S.L. Abergel, V. Apalkov, J. Berashevich, K. Ziegler, T. Chakraborty, Adv. Phys. **59**, 261 (2010)
5. C.L. Kane, E.J. Mele, Phys. Rev. Lett. **95**, 146802 (2005)
6. M. König et al., Science **318**, 766 (2007)
7. S. Raghu, S.B. Chung, X.-L. Qi, S.-C. Zhang, Phys. Rev. Lett. **104**, 116401 (2010)
8. X.-L. Qi, S.-C. Zhang, Rev. Mod. Phys. **83**, 1057 (2011)
9. D. Schmeltzer, A. Saxena, Phys. Rev. B **88**, 239904 (2013)
10. E. Fradkin, Phys. Rev. B **33**, 3263 (1986)
11. E. Fradkin, Phys. Rev. B **33**, 3257 (1986)
12. X. Wan, A.M. Turner, A. Vishwanath, S.Y. Savrasov, Phys. Rev. B **83**, 205101 (2011)
13. J. Smith, S. Banerjee, V. Pardo, W.E. Pickett, Phys. Rev. Lett. **106**, 056401 (2011)
14. A.A. Burkov, L. Balents, Phys. Rev. Lett. **107**, 127205 (2011)
15. A.A. Burkov, M.D. Hook, L. Balents, Phys. Rev. B **84**, 235126 (2011)
16. G. Xu, H. Weng, Z. Wang, X. Dai, Z. Fang, Phys. Rev. Lett. **107**, 186806 (2011)
17. W. Witczak-Krempa, Y.B. Kim, Phys. Rev. B **85**, 045124 (2012)
18. S.M. Young, S. Zaheer, J.C.Y. Teo, C.L. Kane, E.J. Mele, A.M. Rappe, Phys. Rev. Lett. **108**, 140405 (2012)
19. P. Hosur, S.A. Parameswaran, A. Vishwanath, Phys. Rev. Lett. **108**, 046602 (2012)
20. Z. Wang, Y. Sun, X.-Q. Chen, C. Franchini, G. Xu, H. Weng, X. Dai, Z. Fang, Phys. Rev. B **85**, 195320 (2012)
21. B. Singh, A. Sharma, H. Lin, M.Z. Hasan, R. Prasad, A. Bansil, Phys. Rev. B **86**, 115208 (2012)
22. G.Y. Cho, arXiv:1110.1939 (2012)
23. G.B. Halász, L. Balents, Phys. Rev. B **85**, 035103 (2012)
24. R. Nandkishore, D.A. Huse, S. Sondhi, Phys. Rev. B **89**, 245110 (2014)
25. C.-X. Liu, P. Ye, X.-L. Qi, Phys. Rev. B **87**, 235306 (2013)
26. R.R. Biswas, S. Ryu, Phys. Rev. B **89**, 014205 (2014)
27. K. Kobayashi, T. Ohtsuki, K.-I. Imura, Phys. Rev. Lett. **110**, 236803 (2013)
28. Z. Huang, T. Das, A.V. Balatsky, D.P. Arovas, Phys. Rev. B **87**, 155123 (2013)
29. K. Kobayashi, T. Ohtsuki, K.-I. Imura, I.F. Herbut, Phys. Rev. Lett. **112**, 016402 (2014)
30. Y. Ominato, M. Koshino, Phys. Rev. B **89**, 054202 (2014)
31. B. Roy, S. Das Sarma, Phys. Rev. B **90**, 241112(R) (2014)
32. B. Sbierski, G. Pohl, E.J. Bergholtz, P.W. Brouwer, Phys. Rev. Lett. **113**, 026602 (2014)
33. S.V. Syzranov, V. Gurarie, L. Radzihovsky, Phys. Rev. Lett. **114**, 166601 (2015)
34. K. Ziegler, Phys. Rev. Lett. **102**, 126802 (2009)
35. K. Ziegler, Phys. Rev. B **79**, 195424 (2009)
36. M.V. Medvedyeva, J. Tworzydło, C.W.J. Beenakker, Phys. Rev. B **81**, 214203 (2010)
37. P.W. Anderson, Phys. Rev. **109**, 1492 (1958)
38. E. Abrahams, P.W. Anderson, D.C. Licciardello, T.V. Ramakrishnan, Phys. Rev. Lett. **42**, 673 (1979)
39. K. Ziegler, J. Phys. A **45**, 335001 (2012)
40. K. Ziegler, Phys. Rev. B **55**, 10661 (1997)
41. K. Ziegler, Phys. Rev. Lett. **80**, 3113 (1998)
42. K. Ziegler, Eur. Phys. J. B **86**, 391 (2013)
43. D.J. Thouless, Phys. Rep. **13**, 93 (1974)
44. K. Ziegler, Phys. Rev. B **78**, 125401 (2008)
45. A. Sinner, K. Ziegler, Phys. Rev. B **86**, 155450 (2012)
46. N.W. Ashcroft, N.D. Mermin, *Solid State Physics* (Saunders College Publising, 1976)
47. A. Sinner, K. Ziegler, Phys. Rev. B **90**, 174207 (2014)
48. M. Trushin, J. Schliemann, Europhys. Lett. **83**, 17001 (2008)
49. I.M. Lifshits, S.A. Gredeskul, L.A. Pastur, *Introduction to the Theory of Disordered Systems* (Wiley, New York, 1988)
50. S. Villain-Guillot, G. Jug, K. Ziegler, Ann. Phys. **9**, 27 (2000)
51. N.F. Mott, *Metal-Insulator Transitions* (Taylor & Francis, London, 1990)